# IN-PLANE MECHANICAL PROPERTIES OF CF/EPOXY 3-D ORTHOGONAL INTERLOCKED FABRIC COMPOSITE

Naoyuki WATANABE [1], Shigeomi OSHIBA [2], Takashi ISHIKAWA [3]

*[1] Associate Professor, Department of Aerospace Engineering*
*Tokyo Metropolitan Institute of Technology, 6-6 Asahigaoka, Hino-city, Tokyo 191, JAPAN*
*[2] Graduate Student, Department of Aerospace Engineering*
*Tokyo Metropolitan Institute of Technology*
*[3] Section Head, Airframe Division, National Aerospace Laboratory*
*6-13-1 Ohsawa, Mitaka, Tokyo 181, JAPAN*

**SUMMARY**: Tensile tests were executed for obtaining the in-plane mechanical properties of CF/Epoxy 3-D orthogonal interlocked fabric composite. And the prediction of in-plane stiffness, simulation of damage growth and evaluation of ultimate tensile strength are carried out for the models with undulation of in-plane tows by using the 3-dimensional FEM analyses based on the homogenization method. The prediction of damage growth behavior such as transverse crack and delamination is very reasonable, and the predicted stress-strain curve is in good agreement with the experimental results. As for the ultimate failure, the predicted results were considered to be generally in good agreement with the experiments, considering the uncertainty and scatter in the experiments. The present results would give the effective guidelines for predicting the initial failure, damage growth and ultimate tensile strength of this complicated 3-D composites, although more detailed experimental observations were required.

**KEYWORDS:** 3-D Orthogonal Interlocked Fabric Composite, Tensile Test, 3-D FEM Analysis, Homogenization Method, Quadratic Failure Criteria, Damage Growth Simulation

## INTRODUCTION

In comparison with usual 2-D laminated composites, 3-D orthogonal interlocked fabric composites offer many advantages, such as the nature of high interlaminar fracture toughness, notch insensitivity, excellent damage tolerance and great potential of manufacturing cost.

In spite of various developments of elastic stiffness analyses ranging from simplified closed form solution to complicated FEM analysis, there are few works for stress distributions and strength[1)], and even fewer experiments for evaluating the strength.[2)] The main reason why the failure mechanics of 3-D composites is not fully evaluated is their complicated configuration. And strength predictions require the accurate analyses of stress distribution, initiation of transverse crack or delamination and their growth. Furthermore, it should be noted that the

stress concentration is strongly affected by the in-plane tow undulation and the existence of through-the-thickness tows in the strength analyses of 3-D composites.

The object of the present study is to establish a technique for predicting the initial failure, failure growth behavior and the ultimate strength in this composite. In our approach, a geometrical model based on the observation of test specimens is developed first. Next, FEM analysis based on the homogenization method including the thermal effect is adopted to predict elastic properties, stress distributions under uni-axial tensile loading. And, the simulation of damage growth and ultimate strength prediction has been conducted on the basis of predicted detailed stress distributions and appropriate failure criteria.

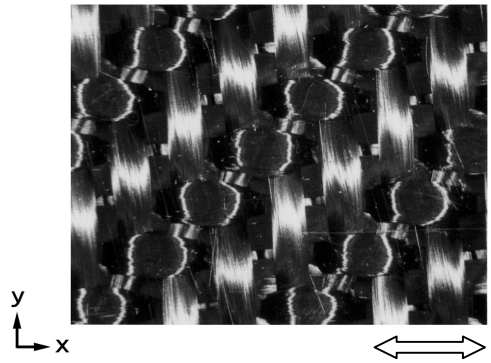


(a) loading direction

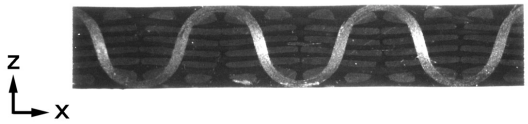


(b)

*Fig.1: Microphotographs of the typical specimen before the test:*
*(a) surface of the specimen*
*(b) filler section of the specimen*

## EXPERIMENT

### Materials

The 3-D orthogonal interlocked fabric composites used in our experiments were made of CF/Epoxy manufactured in Shikijima Bouseki Co. Ltd. It was formed by interlacing 5-layer stuffers, 6-layer fillers and warp weavers, which go through in x-, y- and z-direction, respectively, and each is composed of 3K T300-filaments. To consolidate the composites, resin transfer molding (RTM) technique was adopted. The fiber architecture of 3-D composite is given in Fig. 1(a) and 1(b), and test specimens are 2.52 mm in thickness. It should be noted that in-plane tows of this composite have both in-plane and out-of plane undulation due to warp weaver pressed by through-the-thickness compaction during RTM process, as shown in Fig. 1.

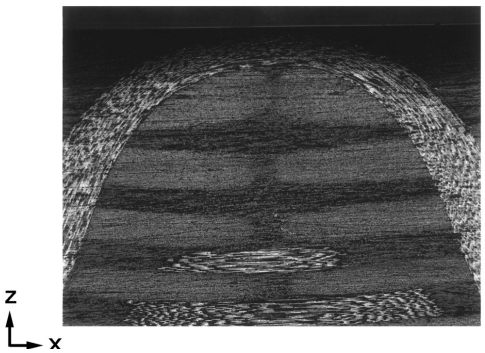


*Fig.2: Microphotograph of polished edge surface before the tensile test*

### Tensile Tests and Observation

Figures 2 and 3 show the polished edge surfaces of specimens before the test. Any visible damage is basically not observed, as shown in Fig. 2. However, it can only be seen that the delamination indicated by the white arrow in Fig. 3 occurs in the region near the surface of specimens where warp weavers wrap around fillers. This failure mode is caused by the thermal expansion mismatch of three kinds of tows.

Static Tensile tests were executed to obtain in-plane mechanical properties and the number of specimens parallel to the x-axis is six, and acoustic emission signals are monitored during the test.

The averaged values of obtained material

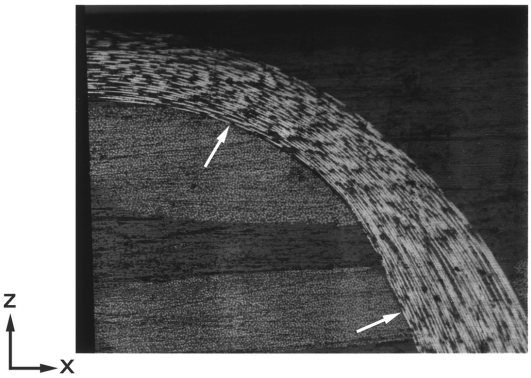


*Fig.3: Delamination on polished edge surface before the tensile test*

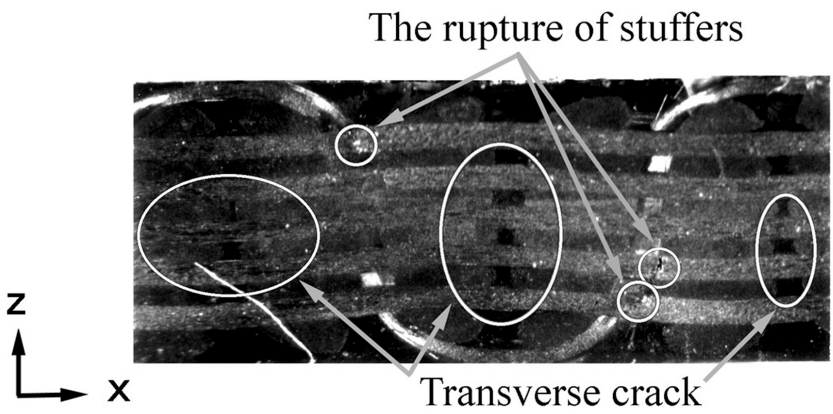


*Fig.6: Microphotograph of the typical specimen after the test*

properties from the tensile test and analytical ones are summarized in Table 1. As for initial Young's modulus $E_x$, the maximum, minimum and averaged values are 38.46GPa, 37.23GPa and 37.92GPa, respectively, and then the scatter is very small. On the other hand, for the tensile strength the maximum, minimum and averaged values are 524.4MPa, 449.3MPa, and

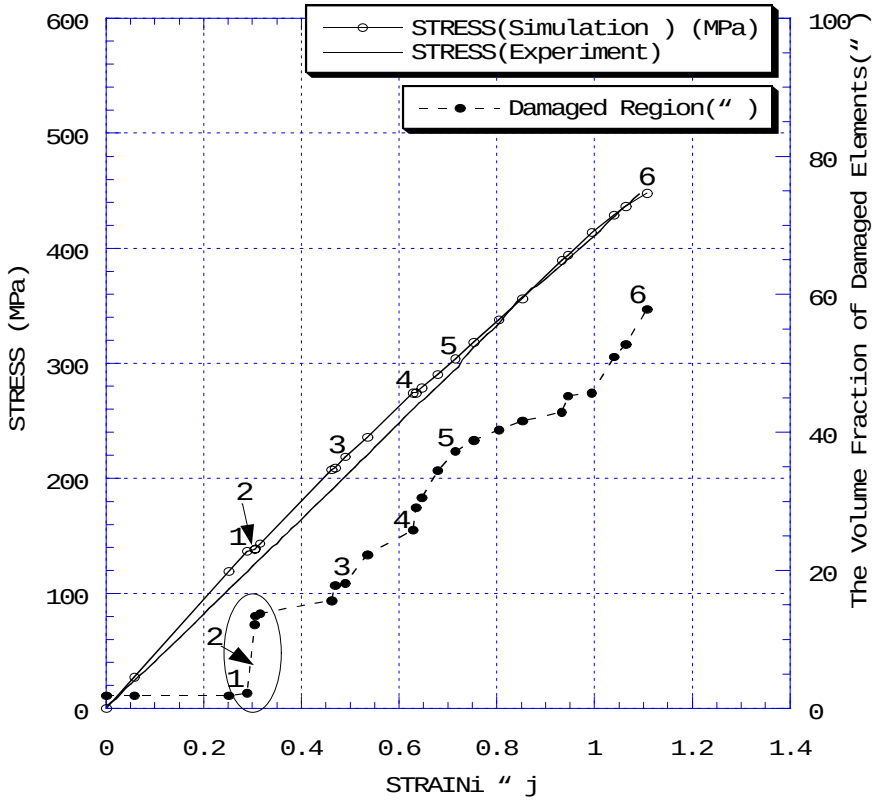


*Fig.4: Experimental and theoretical stress-strain curves and the relation between the volume fraction of damaged region and strain*

472.6MPa, respectively, and it leads to large scatter. Figure 4 denotes the tensile stress-strain curve for a typical specimen, and the relation between AE total count and strain is given in Fig. 5. The simple solid line indicates the experimental curve, and it is nearly linear, and any knee point can not be seen. Instead of the knee point, the nonlinear behavior can be seen near the strain of approximately 0.7%, which coincides with the stress of 300MPa. Furthermore, this onset of nonlinear behavior corresponds with the area surrounded by the circle in the graph between AE total count and strain relation.

Figure 6 shows the microphotograph of the typical specimen after the test. In this figure, the rupture of stuffer along the loading direction is found near the crossover point of stuffer and warp weaver surrounded by white circles, owing to the in-plane undulation of stuffers caused by the existence of warp

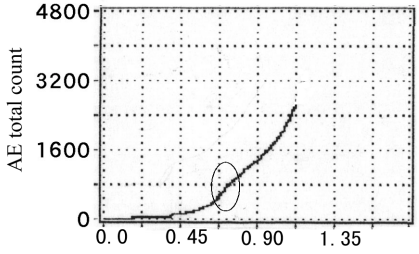

weaver. It is also observed that transverse cracks occur in the stuffers put between resin rich regions.

*Table 1: Experimental and analytical results of in-plane mechanical properties*

| | Initial Young's modulus *Ex* (GPa) | Initial in-plane share modulus *Gxy* (GPa) | Tensile strength (MPa) | Failure strain (%) |
|---|---|---|---|---|
| Exp. | 37.92 | 3.03 | 472.6 | 1.14 |
| Model A | 37.02 (-2.4%) | 3.02 (-0.3%) | - | - |
| Model B | 40.45 (+6.7%) | 3.14 (+3.6%) | 447.9 (-5.2%) | 1.11 (-2.6%) |

## MODIFIED FEM ANALYSIS

### Modeling of 3D-woven Composites

Since in-plane tows have both in-plane and out-of-plane undulation as mentioned before, it is important to consider their effects in predicting composite behavior, especially for initial failure strength, ultimate tensile strength and damage growth. Here, two kinds of models are considered in our analyses as mentioned below.

Based on the observed detailed geometry of the test specimens as shown in Fig. 1, "Model A" is constructed as shown in Fig. 1. It is assumed that the in-plane trajectory of in-plane tow is sinusoidal curve and stuffers have both in-plane and out-of-plane undulation, but that fillers have only in-plane undulation for the simplicity. As indicated in Fig. 1, the wavelength of out-of-plane undulation is twice as long as that of in-plane undulation. Figure 7 shows the configuration of this unit cell and the finite element mesh.

As for "Model B", the in-plane tows have only in-plane undulation and other geometrical parameters are completely the same as those of Model A. Therefore, the unit cell size of this model is half of Model A and its in-plane shape is square. The configuration parameters of the both models are given in Table 2.

The size and fiber volume fraction of each tow are determined, considering the architectures of each tow, the amount of fibers per tow is 3K filaments and total volume fraction of this composite $V_{fc}$ is 42.6%. Detailed thermo-elastic properties of each tow are given in Tables 3 and 4. One of authors indicated that the unidirectional carbon composites exhibit significant hardening in longitudinal tension due to the nature of carbon fiber.[3)] According to the results in Ref. 2, the longitudinal modulus of carbon fiber at lower stress level is 20% lower than the higher stress. Therefore, in order to compare with the experimental stiffness in Table 1, the initial elastic properties of each tow are adopted as shown in Table 3. On the other hand, to simplify the damage growth analysis, this material nonlinearity is not included. Consequently, the elastic properties of each tow in Table 4 are adopted in the damage growth analysis.

*Table 2: Configuration parameters in the Model A and B*

| | Undulation $a_i$ (mm)[#] $a_o$(mm)[#] | $V_{fc}$ (%) | $V_{fs}$&$V_{ff}$ (%) | $V_{fw}$ (%) | Width of unit cell: $\lambda_x$ (mm) | Depth of unit cell: $\lambda_y$ (mm) | Height of unit cell: $\lambda_z$ (mm) |
|---|---|---|---|---|---|---|---|
| Model A | 0.0735(in-plane) 0.116(out-of-plane) | 42.6 | 48.3 | 75.6 | 5.09 | 2.55 | 0.46 |
| Model B | 0.0735(in-plane) | | | | 2.55 | | |

[#]: $a_i$, $a_o$: Amplitudes of in-plane and out-of-plane undulation, respectively

*Table 3: Thermo-elastic properties of each tow at lower stress level*

| Tow | $E_L$ (GPa) | $E_T$ (GPa) | $G_{LT}$ (GPa) | $G_{TT}$ (GPa) | $\nu_{LT}$ | $\nu_{TT}$ | $\alpha_L$ (1/K) | $\alpha_T$ (1/K) |
|---|---|---|---|---|---|---|---|---|
| in-plane tow | 93.3 | 7.32 | 3.32 | 2.41 | 0.35 | 0.52 | $5.20\times10^{-7}$ | $4.68\times10^{-5}$ |
| warp weaver | 144.3 | 11.5 | 7.70 | 3.95 | 0.33 | 0.47 | $-3.72\times10^{-7}$ | $2.55\times10^{-5}$ |

*Table 4: Thermo-elastic properties of each tow at high stress level*

| Tow | $E_L$ (GPa) | $E_T$ (GPa) | $G_{LT}$ (GPa) | $G_{TT}$ (GPa) | $\nu_{LT}$ | $\nu_{TT}$ | $\alpha_L$ (1/K) | $\alpha_T$ (1/K) |
|---|---|---|---|---|---|---|---|---|
| in-plane tow | 115.4 | 7.34 | 3.33 | 2.41 | 0.35 | 0.53 | $2.68\times10^{-7}$ | $4.68\times10^{-5}$ |
| warp weaver | 178.6 | 11.5 | 7.70 | 3.95 | 0.33 | 0.47 | $-4.50\times10^{-7}$ | $2.26\times10^{-5}$ |

**Analytical Method**

In the analysis, extended homogenization method with considering thermal effect has been developed and applied to 3-D composites. A temperature drop during RTM process is assumed to be 100K, and these models are subjected to uni-axial tensile load, where loading direction is parallel to the x-axis. After the obtained stress components are averaged in each finite element, the failure can be predicted, based on the stress and following quadratic failure criteria by checking each finite element in the unit cell.

Tsai-Wu quadratic failure criterion are applied to each tow in conjunction with the strength ratio, *R* defined as the ratio of the initial failure strength to the applied stress in order to predict the damage growth, and *R* is computed as the following equation in respect with each element. [4)]

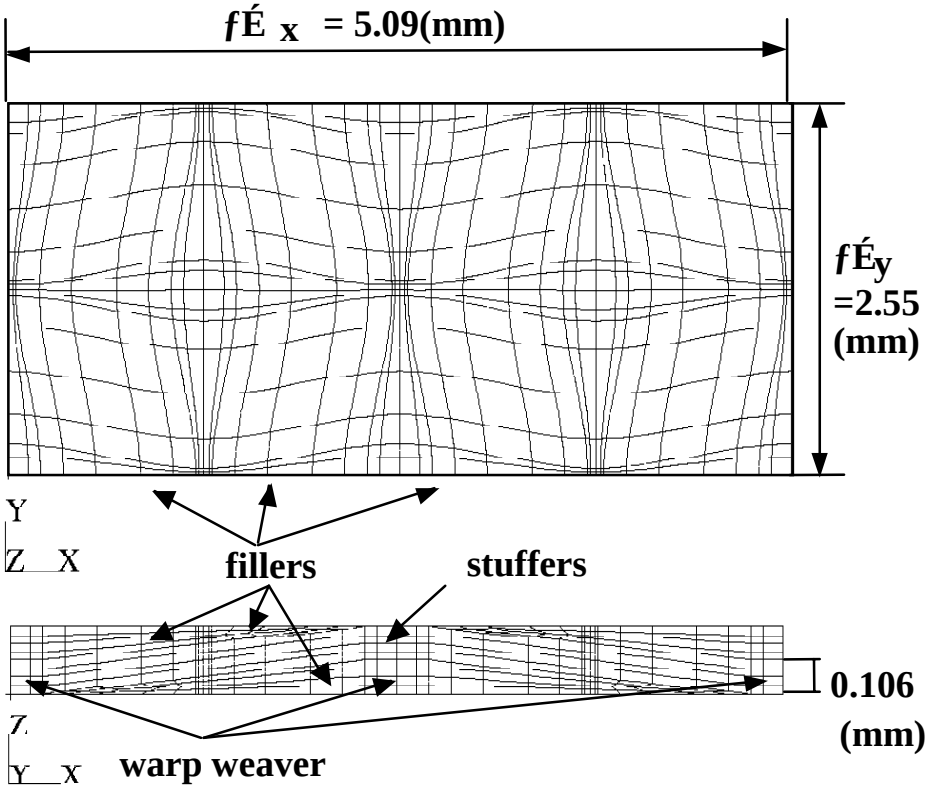


*Fig. 7: Configuration and finite element mesh of Model A*

$$R^2\left(F_{ij}\sigma^a_i\sigma^a_j\right)+R\left(F_i\sigma^a_i+F_{ij}\sigma^a_i\sigma^T_j\right)+F_{ij}\sigma^T_i\sigma^T_j+F_i\sigma^T_i=1 \quad (i,j=1\sim6) \tag{1}$$

where $F_{ij}$ (i, j=1~6) are strength parameters. $\sigma^a_i$ is stress when the unit cell is subjected to unit averaged stress, and $\sigma^T_i$ is residual stress due to the temperature drop. Similarly, Von-Mises criterion is adopted in the epoxy region. The minimum value $R_{min}$ is obtained by comparing with all values of $R$. Here, we introduce the normalized value $R_n$ which is $R$ / $R_{min}$ for each element. Although the material is damaged when $R_n$ is equal to unity, it is assumed to be damaged when $R_n$ is greater than 0.95, considering sequential damage growth. If these criteria are fulfilled, the elastic property of each element is reduced as follows. The transverse and shear stiffness of the tow elements become 1/100 and 1/5 of each initial value, while the all stiffness components of predicted epoxy elements are reduced to 1/100. And then the load is increased again, and the damage growth analysis in the above is repeated until the ultimate failure of the unit cell occurs. If the fiber breakage occurs in the stuffers, the composite is assumed to suffer ultimate failure. As for the prediction of fiber breakage, maximum stress criterion is applied to each element instead of the Tsai-Wu criterion.[5)]

**Determination of strength parameters**

The longitudinal tensile strength ($F_{LT}$) is determined by considering the fiber volume fraction of each tow and the strength of CFRP unidirectional lamina. It is very difficult but important to estimate the transverse tensile strength ($F_{TT}$) of each tow in order to predict the initial failure and damage growth, but it is also difficult because of constraint effect and the existence of voids, etc.[6),7)] Therefore, it is assumed that the onset of AE signals during the tests is regarded as the transverse crack initiation of fillers. Since the value of AE onset is approximately 0.4% in Fig. 5, the $F_{TT}$ value of stuffers and fillers in the Tsai-Wu criterion is determined to be 80MPa. This is the maximum value of $\sigma_x$ in fillers, when Model A is subjected to the averaged strain 0.4% parallel to the x-direction. On the other hand, it is assumed that warp weavers have been already damaged since it is considered that the delamination propagates unstably from the crack tip near the surface as observed in Fig. 3. Therefore, the $F_{TT}$ value of this tow is determined to be 87MPa. The interlaminar tensile strength of all tows is assumed to be equal to transverse tensile strength $F_{TT}$. The estimated strength properties of each tow and epoxy are given in Table 5

*Table 5: Strength properties of each tow and epoxy*

| material | $F_{Lt}$ (GPa) | $F_{Lc}$ (GPa) | $F_{Tt}$ (GPa) | $F_{Tc}$ (GPa) | $S_{LT}$ (GPa) | $S_{TT}$ (GPa) |
|---|---|---|---|---|---|---|
| in-plane tow | 1.35 | 1.49 | 0.80 | 0.28 | 0.093 | 0.093 |
| warp weaver | 2.06 | 1.49 | 0.87 | 0.28 | 0.093 | 0.093 |
| #828 epoxy | 0.089 | 0.089 | 0.089 | 0.089 | - | - |

## RESULTS AND DISCUSSION

### Evaluation of Stiffness and Stress Distribution in both models

Experimental and theoretical results of stiffness are compared in Table 1. The initial Young's modulus and in-plane shear modulus of Model A are in good agreement with experimental results, while analytical results of Model B are a little different from experimental ones. Consequently, it is very important to consider not only the effect of the in-plane tow undulation but also the material nonlinearity of carbon fiber in order to predict initial in-plane stiffness.

Figures 8 and 9 indicate $\sigma_x$ and $\sigma_y$ stress distributions in the stuffers when each model is subjected to the averaged ultimate tensile load obtained in the experiments. Figure 8 shows that stress concentrations in both models occur at the regions surrounded by circles and they are around warp weavers in the stuffers. It is because the bending stress is caused by the in-plane undulation of the stuffers. Although Model A has also out-of-plane undulation unlike Model B, stress distributions in the both models are very similar to each other especially for $\sigma_y$ stress distribution shown in Fig. 9. Consequently, damage growth analysis is only carried out for Model B for the simplicity.

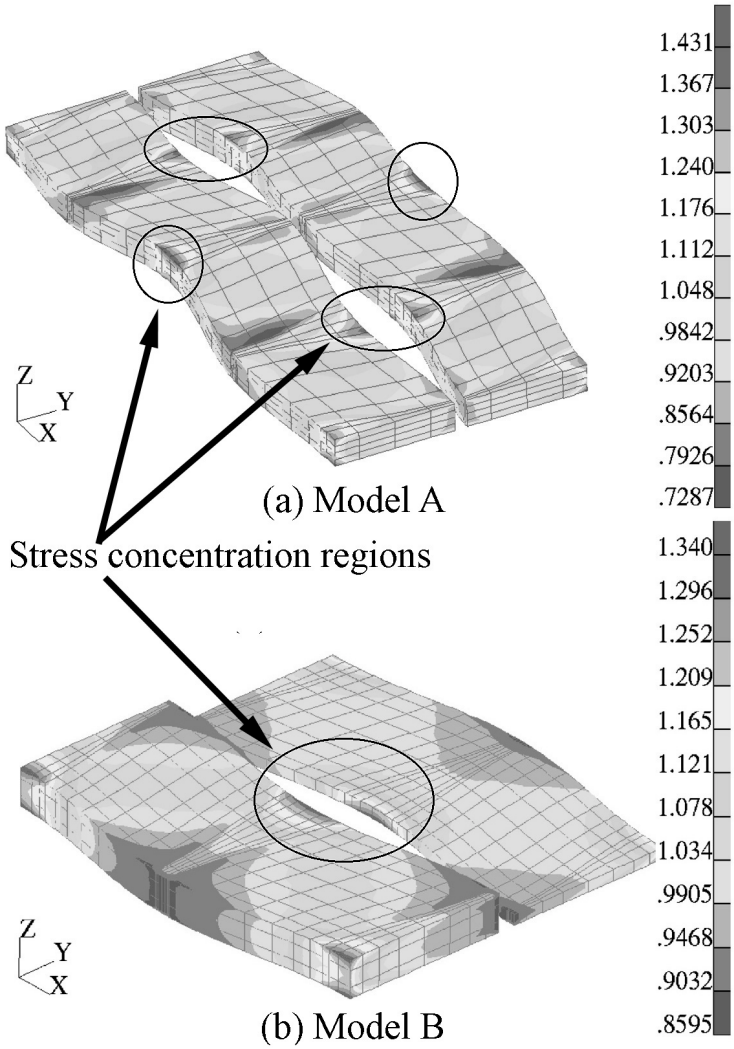


*Fig. 8: $\sigma_x$ stress distribution in the stuffers when The experimental tensile load is applied to Model A & B*

**Damage Growth Analysis**

The damage growth analysis of Model B is performed without consideration of the longitudinal nonlinear property of carbon fiber. Figure 4 indicates experimental and theoretical stress-strain curves and the relation between the volume fraction of damaged region and strain. A solid line with circular symbols denotes a predicted stress-strain curve, and a dashed line denotes the volume fraction of damaged elements with respect to strain. Although the volume fraction of damaged region amounts to 58% at the ultimate failure, the stress-strain curve is approximately linearity. The analytical stress-strain curve is very close to the experimental one at higher stress level, while it departs from the experimental result at lower stress level. The main reason of the difference at lower stress level is neglecting the effect of material nonlinearity, and it would be only a little influence on predicting the ultimate strength. The volume of damaged elements is predicted to reach 74% in stuffers and 61% in fillers when the ultimate failure is predicted by maximum stress criterion. And predicted final Young's moduli, $E_x$ and $E_y$, are reduced to 40.5GPa and 41.0GPa. As given in Table 1, the experimental strength and failure strain are slightly larger than predicted ones, and errors of both values are 5.2% and 2.6%. Consequently, it is considered that this FEM simulation can predict the actual behavior of the 3-D composite to a high degree, when we consider the scatter of strength in the experiments.

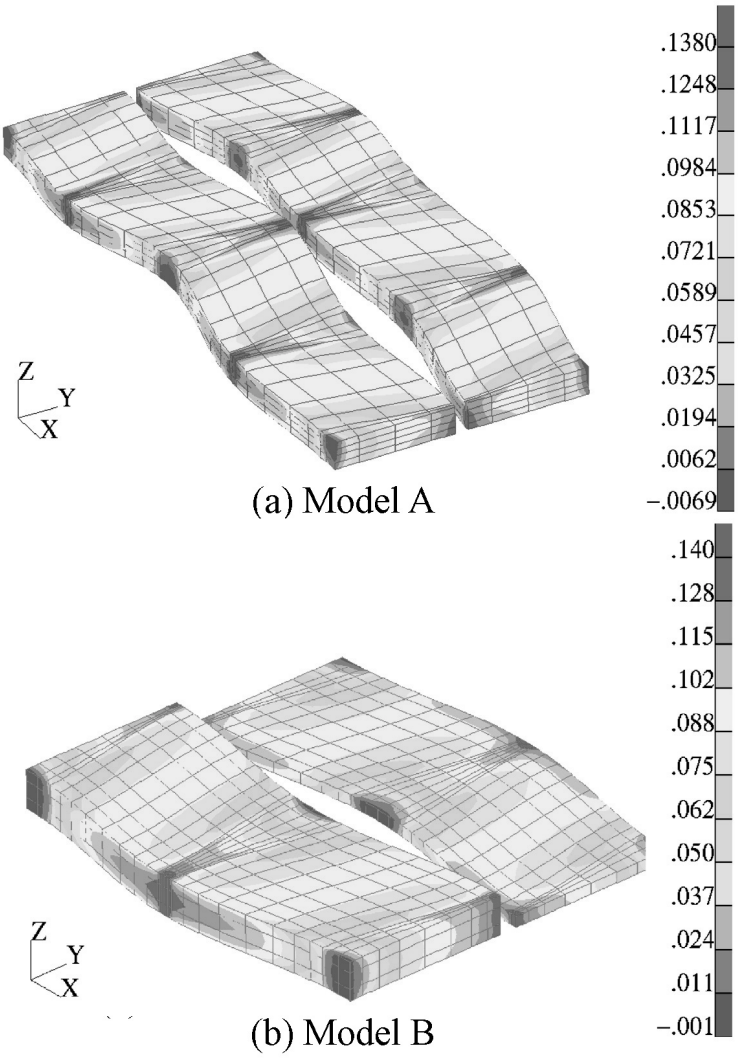


*Fig. 9: $\sigma_y$ stress distribution in the stuffers when The experimental tensile load is applied to Model A & B*

The numbers indicated in Fig. 4 correspond to each step of damage growth in Figs. 9 and 10. The predominant failure mode in each failure step is discussed below. Figure 10 illustrates the damaged elements in fillers propagates gradually, and especially drastic damage growth propagates along the fiber direction only in fillers between steps 1 and 2 at the strain of 0.3%. This failure mode is regarded as transverse crack dominated mainly by the magnitude of $\sigma_x$ and it continues to make gradual progress up to step 4. And then the interfacial debonding is caused by mainly by $\sigma_z$ and $\tau_{xz}$, and it propagates along the interface between the fillers and stuffers.

In Fig. 11, the damage propagation in stuffers at each step is illustrated. It is noted that the failure propagation begins at step 2 in Fig. 4 and 11. This failure mode is regarded as transverse crack and makes gradual growth along the fiber direction until step 4. At the same time, interfacial debonding in fillers is induced in Fig. 10 and it propagates between in-plane

tows. Finally, the rupture of stuffer occurs around the warp weavers where stress concentration regions are indicated in Fig. 8. Furthermore, the predicted damage morphology is similar to that of CF/Epoxy cross-ply laminates. [7)]

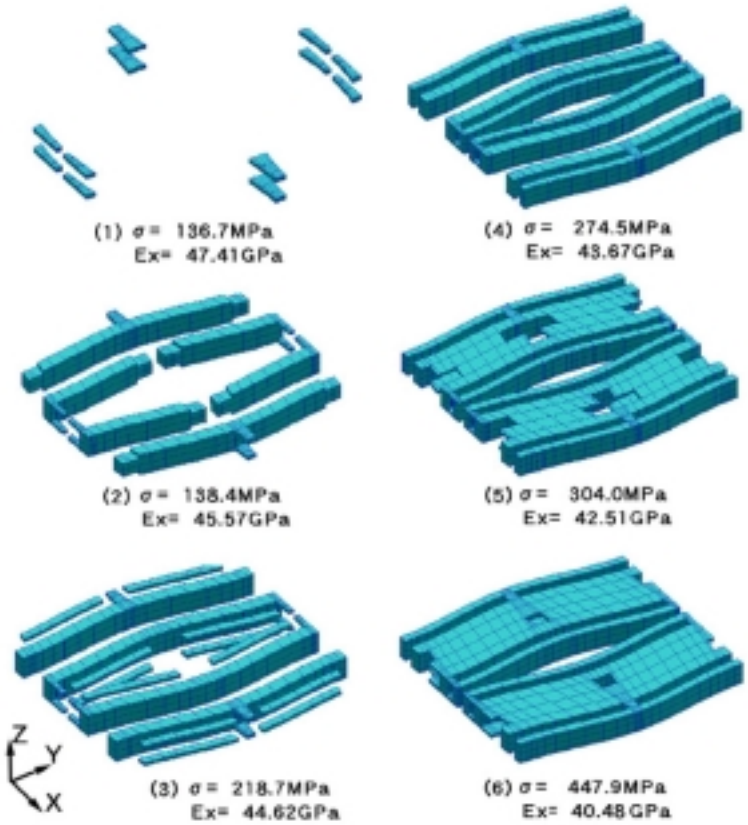


*Fig. 10: Damage growth in fillers*
*(These steps of damage propagation correspond to each step in Fig.4)*

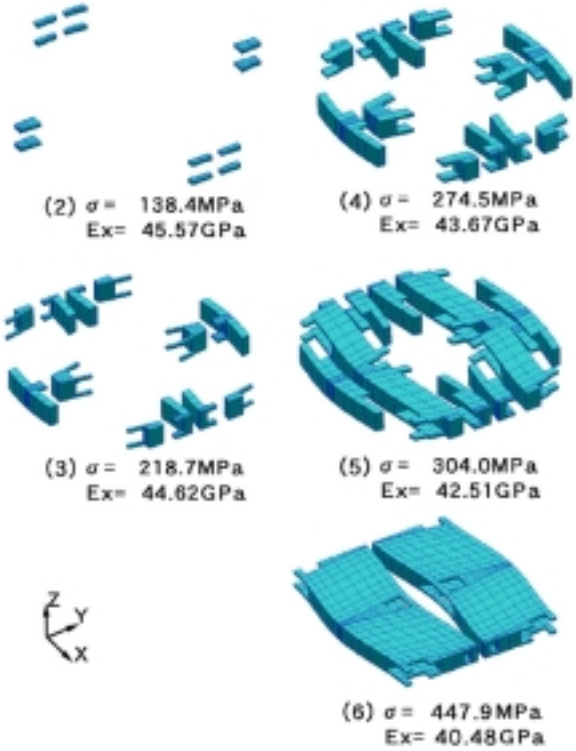


*Fig. 11: Damage growth in stuffers*
*(These steps of damage propagation correspond to each step in Fig.4)*

## CONCLUSION

In-plane mechanical properties of the CF/Epoxy 3-D orthogonal interlocked fabric composite were evaluated by both of the experiment and analysis. In the analysis, 3-dimensional FEM simulation program has been developed based on the homogenization method with including thermal effect and undulation of in-plane tows. The conclusions are given as follows:

1) The initial Young's modulus and in-plane shear modulus of Model A were in good agreement with experimental results, while analytical results of Model B were fairly good agreement with experimental ones. Therefore, it was very important to consider not only the effect of the in-plane tow undulation but also the material nonlinear response of carbon fiber in order to predict initial in-plane stiffness.
2) We have developed the analytical technique for predicting the fundamental failure mode and damage growth. The predicted damage morphology is as follows: First, transverse cracking initiates and drastic damage growth propagates in the fillers. In the next step, the same damage behavior makes gradual growth in stuffers. At high stress level, interfacial debonding occurs and propagates between stuffers and fillers. Therefore, the predicted stress-strain curve is in good agreement with the experimental results.
3) As for the ultimate failure, the predicted results were considered to be generally in good agreement with the experiments, considering the uncertainty and scatter in the experiments. Consequently, the present results would give the effective guidelines for predicting the initial failure, damage growth and ultimate tensile strength of this complicated 3-D composites, although more detailed experimental observations were required.

## REFERENCES


1. John, S., Coman, F., Bannister, M., and Hersxberg, I., "A Theoretical Framework for the Consideration of Damage Entities in 3D Woven Composite Structures," *Proceedings of ICCM-11*, Gold Coast, Australia, July, 1997, pp. V377-V383.

2. Cox, B.N., Dadkhah, W.L., Morris, W.L., and FLINTOFF, J.G., "Failure Mechanisms of 3D Woven Composites in Tension, Compression, and Bending," *Acta metall. Mater.*, Vol. 42, No. 12, 1994, pp. 3967-3984.

3. Ishikawa, T., and Matsushima, M., and Hayashi. Y., "Geometrical and Material Nonlinear Properties of Two-Dimensional Fabric Composites," *AIAA Journal*, Vol. 25, No.1, 1987, pp. 107-113.

4. Kim, R.Y., "Initiation of Free-edge Delamination in Composite Laminates," *Key Engineering Materials*, Vol. 37, 1989, pp. 103-136.

5. Zhu, H. and Sankar, B.V., "Evaluation of Failure Criteria for Fiber Composites Using Finite Element Micromechanics," *Jounal of Composite Materials*, Vol.32, No.8, 1998, pp.766-782.

6. Fraggs, D.L. and Kural, M.H., "Experimental Determination of the In Situ Transverse Lamina Strength in Graphite/Epoxy Laminates," *Jounal of Composite Materials*, Vol.16, 1982, pp.103-116.

7. Takeda, N. and Ogihara, S., "Initiation and Growth of Delamination from the Tips of Transverse Cracks in CFRP Cross-ply Laminates," *Composites Science and Technology*, Vol.52, 1994, pp.309-318.